Analytica Chimica Acta 906 (2016) 148–155

Contents lists available at ScienceDirect

Analytica Chimica Acta

journal homepage: www.elsevier.com/locate/aca

Highly photoluminescent MoO_x quantum dots: Facile synthesis and application in off-on Pi sensing in lake water samples

Sai Jin Xiao [a, b], Xiao Jing Zhao [b], Jun Zuo [b], Hai Qing Huang [c], Li Zhang [d, *]

[a] Jiangxi Key Laboratory of Mass Spectrometry and Instrumentation, East China University of Technology (ECUT), Nanchang 330013, China
[b] School of Chemistry, Biology and Material Science, ECUT, Nanchang 330013, China
[c] State Key Laboratory Breeding Base of Nuclear Resources and Environment, ECUT, Nanchang 330013, China
[d] College of Chemistry, Nanchang University, Nanchang 330031, PR China

HIGHLIGHTS

- Though increasing effort has been devoted to MoO_x nanomaterials synthesis, only a few reports mentioning its photoluminescence property are available, while even no evidence has shown its applications in chemical and biological sensing.
- Herein, a one-pot method possessing the advantages of rapid, easily prepared and environment friendly was developed for facile synthesis of highly photoluminescent MoO_x quantum dots, which was further utilized to construct a new off-on sensor for phosphate determination in complicated lake water samples.

GRAPHICAL ABSTRACT

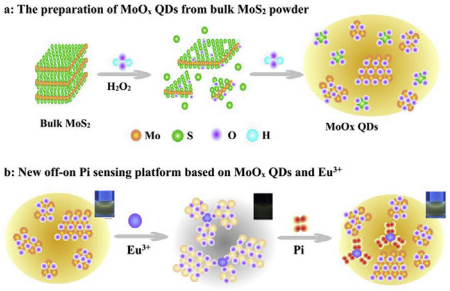

ARTICLE INFO

Article history:
Received 28 October 2015
Received in revised form
2 December 2015
Accepted 12 December 2015
Available online 18 December 2015

Keywords:
Molybdenum oxide quantum dots
Photoluminescence
Eu^{3+}
Pi

ABSTRACT

Molybdenum oxide (MoO_x) is a well-studied transition-metal semiconductor material, and has a wider band gap than MoS_2 which makes it become a promising versatile probe in a variety of fields, such as gas sensor, catalysis, energy storage ect. However, few MoO_x nanomaterials possessing photoluminescence have been reported until now, not to mention the application as photoluminescent probes. Herein, a one-pot method is developed for facile synthesis of highly photoluminescent MoO_x quantum dots (MoO_x QDs) in which commercial molybdenum disulfide powder and hydrogen peroxide (H_2O_2) are involved as the precursor and oxidant, respectively. Compared with current synthesis methods, the proposed one has the advantages of rapid, one-pot, easily prepared, environment friendly as well as strong photoluminescence. The obtained MoO_x QDs is further utilized as an efficient photoluminescent probe, and a new off-on sensor has been constructed for phosphate (Pi) determination in complicated lake water samples, attributed to the fact that the binding affinity of Eu^{3+} ions to the oxygen atoms from Pi is much higher than that from the surface of MoO_x QDs. Under the optimal conditions, a good linear relationship was found between the enhanced photoluminescence intensity and Pi concentration in the range of 0.1 −160.0 μM with the detection limit of 56 nM (3σ/k). The first application of the photoluminescent MoO_x nanomaterials for ion photochemical sensing will open the gate of employing MoO_x nanomaterials as versatile probes in a variety of fields, such as chemi-/bio-sensor, cell imaging, biomedical and so on.

* Corresponding author.
E-mail address: zhangli8@ncu.edu.cn (L. Zhang).

http://dx.doi.org/10.1016/j.aca.2015.12.022
0003-2670/

1. Introduction

Molybdenum trioxide (MoO_x) nanomaterials, a well-studied transition-metal semiconductor material, have been widely applied in gas sensors [1,2], photochromism [3], catalysis [4], lithium-ion batteries [5], field effect transistors [6], antibacterial and anticancer [7,8], ect. Recently, increasing effort has been devoted to the synthesis of MoO_x nanomaterials with different morphology as the chemical properties of MoO_x nanomaterials changes dramatically with the morphology. Unitl now, various morphology including nanobelt [9,10], nanoflower [11], nanosheets [4,12,13], nanoflake [14], nanorod [5], nanowire [15], nanoplate [8] and nanoribbon [16] etc have been successfully prepared *via* hydrothermal/solvothermal method [12,15], chemical spray pyrolysis [17], thermal evaporation and decomposition [8], mechanical grinding and sonication [5,16], nanosecond-duration plasma discharges technique [18], and electrospinning [19]. However, almost all of the above methods are time-consuming, demanding tedious procedure or requiring external stimuli such as lasing, shear, evaporation, decomposition, sonication, grinding and heating. Moreover, only a few reports mentioning the photoluminescence property of MoO_x nanomaterials are available [1,7,20,21], in which the MoO_x nanomaterials are mostly deposited on thin film and the fluorescence quantum yield is usually insufficient, while even no evidence has shown its applications as fluorescence probes in chemical and biological sensing. On this line, development of a rapid, one-pot and environmentally friendly methods for the large-scale synthesis of photoluminescent MoO_x nanomaterials and its further application are still challenging.

In this manuscript, a one-pot method was developed for facile synthesis of photoluminescent MoO_x quantum dots (MoO_x QDs). Commercial molybdenum disulfide powder was employed as the precursor, and hydrogen peroxide (H_2O_2) which is capable to promote and even enhance the oxidization/reduction state of the ablated molybdenum clusters [22], was involved as the oxidant. Compared with other synthesis methods, the present one demonstrates great advantages. Firstly, the synthesis is rapid and one-pot, and MoO_x QDs can be obtained in 1 h or less. Secondly, the reaction is performed at room temperature without any external stimuli. Thirdly, and also the most important one, the as-prepared MoO_x QDs has strong photoluminescence which is comparable to that of graphene quantum dots, carbon dots and MoS_2 QDs [23–25], and the absolute fluorescence quantum yield is 1.35%.

The as-prepared MoO_x QDs were further utilized to construct a new off-on photoluminescence sensor for phosphate (Pi) determination. Pi is an essential component in the nutritional chain of aquatic microorganisms, and has been considered as a convenient indicator or tracer of organic pollution in bodies of water [26]. Scheme 1 shows the construction of Pi sensing platform using photoluminescent MoO_x QDs and Eu^{3+} ions. Firstly, Eu^{3+} is able to quench the photoluminescence of MoO_x QDs since Eu^{3+} displays a certain affinity to oxygen atoms and acts as a bridge to link the neighboring MoO_x QDs (turn-off). On the other hand, Eu^{3+} has higher affinity to the oxygen atoms originated from Pi than that from the surface of MoO_x QDs, leading to the disassociation of MoO_x QDs-Eu^{3+} complexes in the presence of Pi and the restoration of photoluminescence (turn-on). With the present off-on sensing platform, Pi in lake water samples could be rapidly and selectively detected without tedious sample pretreatment processes, and the accuracy and repeatability are acceptable for Pi detection in complicated samples.

2. Experimental section

2.1. Chemicals and reagents

MoS_2 powder, leucine (Leu), BSA and amylase (Amy) were commercially from Sigma-Aldrich (USA). $Eu(NO_3)_3$ (99.99%), anions (SO_4^{2-}, SO_3^{2-}, S^{2-}, ClO^-), metal ions (Zn^{2+}, Cu^{2+}, Hg^{2+}, Fe^{2+}, Co^{2+}, Cd^{2+}, Ni^{2+}, Mn^{2+}) were purchased from Shanghai Maikun Chemical Reagents Co. Ltd (Shanghai, China). Sodium phosphate was from Sinopharm Chemical Reagents Co. Ltd, (Shanghai, China). All chemicals and solvents were analytical grade and were used without further purification. Deionized water was used throughout.

2.2. Apparatus and characterization

A JEOL Ltd JEM-2010 transmission electron microscope (TEM; Japan) with a 200 kV accelerating voltage and a Bruker MultiMode 8 atomic force microscope by the ScanAsyst mode were utilized to measure the size and height of MoO_x QDs, respectively. The elemental composition and bonding configuration characterization was measured by X-ray photoelectron spectroscopy (XPS) (Thermo, USA), the absolute fluorescence quantum yield was recorded by Quantaurus-QY absolute quantum yield spectrophotometer (Hamamatsu, Japan), and Fourier transform infrared spectra (FTIR) were obtained on a Nicolet 5700 FTIR spectrometer (Nicolet). A Shimadzu UV-2450 spectrophotometer (Tokyo, Japan) and a Hitachi F-7000 fluorescence spectrophotometer (Tokyo, Japan) or USB-4000FL spectrophotometer (Ocean Optical, U.S.A) were employed to measure the absorption and fluorescence spectra, a FL-TCSPC fluorescence spectrophotometer (Horiba Jobin Yvon Inc, France) was used to record the fluorescence lifetime.

2.3. Synthesis of MoO_x QDs

The MoO_x QDs were synthesized from commercial MoS_2 powder (99% purity, Sigma Aldrich). Briefly, 10.0 mg MoS_2 powders were added into 6.0 mL H_2O and 4.0 mL 30% H_2O_2, stand at room temperature for 30 min, and the pH of the mixture were then ajusted to 7.0 with sodium hydroxide (NaOH). Finally, the MoO_x QDs was obtained by centrifugation at 8000 g for 10 min.

2.4. Quenches the fluorescence of MoO_x QDs with Eu^{3+}

The quenching of the fluorescence of MoO_x QDs with Eu^{3+} was performed as followed: Tris–HCl buffer (20 μL 50 mM, pH 7.5), MoO_x QDs (20 μL, 1 mg/mL), different concentrations of Eu^{3+} and deionized water were added into a centrifuge tube, and immediately mixed thoroughly on the vortex mixer. The fluorescence spectra of the resulting solution were recorded on the USB-4000FL spectrophotometer by excitation at 405 nm after incubation of 10 min.

2.5. Pi detection by MoO_x QDs and Eu^{3+}

For the Pi sensing experiments, Tris–HCl buffer (50 mM, pH 7.5), MoO_x QDs (20 μL, 1 mg/mL), Eu^{3+} (20 μL, 2.75 μM), different concentrations of Pi solution and deionized water were added into a centrifuge tube, and immediately mixed thoroughly on the vortex mixer. The fluorescence spectra of the resulting solution were recorded on the USB-4000FL spectrophotometer by excitation at

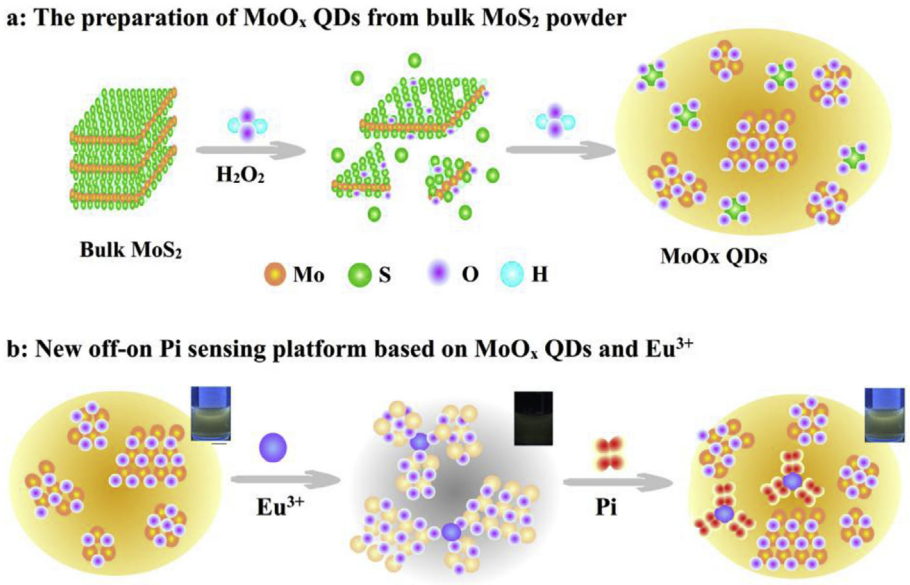

Scheme 1. Preparation of MoO_x QDs from bulk MoS_2 powder (a) and the construction of new off-on Pi sensing platform using photoluminescent MoO_x QDs and Eu^{3+} ions (b).

405 nm after incubation of 10 min.

3. Results and discussion

3.1. Characterization of the MoO_x QDs

As a new type of nanomaterial, the morphology and surface chemical properties of the as-prepared MoO_x QDs were investigated in detail, as shown in Fig. 1. Quantitative analysis of the diameter of MoO_x QDs was performed by measuring 100 individual particles from multiple TEM images, and the average diameter was about 4.4 nm (Fig. 1a and Fig. S1). Atomic force microscopic (AFM) imaging was also achieved to characterize the morphology of MoO_x QDs, in which the height was about 2.1 nm (Fig. 1b). The surface chemical property of the as-prepared MoO_x QDs were measured by X-ray photoelectron spectroscopy (XPS), and Mo3d, S2p, O1s and Na1s peaks were obtained in the survey spectrum (Fig. 1c), which were further characterized from the high-resolution XPS (Fig. 1d, e). Both the Mo3d and S2p doublets were shifted to the higher binding energy pair, while the S2s peak disappeared compared with that of MoS_2 powder (Fig. 1d, e and Fig. S2), indicating the oxidation of MoS_2 by H_2O_2 which is in accordance with other reports [27]. The spectrum of Mo3d showed four peaks at 231.7, 234.9 eV, 232.8 and 236.3 eV corresponding to Mo^{5+} $3d_{5/2}$, Mo^{5+} $3d_{3/2}$, Mo^{6+} $3d_{5/2}$, and Mo^{6+} $3d_{3/2}$, respectively (Fig. 1d) [28,29]. On the basis of the XPS peak area of Mo 3d, the proportion of Mo^{5+} and Mo^{6+} in the obtained MoO_x QDs was 67.0% and 36.0%, respectively, and the average oxidation state of Mo was thus calculated to be 5.33, which was obviously the mixed-valence state account for the oxygen vacancies. The S $2p_{3/2}$ and S $2p_{1/2}$ peaks at 168.5 and 169.7 eV were identified as the S2p peaks of oxidized sulphur (SO_4^{2-}) (Fig. 1e) [25,29,30], and the peaks of the oxidized sulphur were disappeared when MoO_x QDs was dialysis for 48 h in ddH_2O (Fig. S3), suggesting that almost all of S^{2-} were oxidized by H_2O_2 and the oxidized sulphur were free in the solution. Taking together, it can be clearly concluded that the as-prepared MoO_x QDs was a combination of MoO_3 and Mo_2O_5, and MoS_2 might be oxidized by H_2O_2 according to the reaction in Equation (1).

$$6MoS_2 + 25H_2O_2 \rightarrow 2MoO_3 + Mo_2O_5 + 12SO_4^{2-} + 24H^+ + 13H_2O \quad (1)$$

In a word, it can be clearly concluded that the S^{2-} and Mo^{4+} were converted to the higher oxidation states (S^{6+}, Mo^{5+} and Mo^{6+}) when MoS_2 were spontaneously exfoliated and oxidized by H_2O_2 [31]. During the oxidation process, more and more S atoms were released from the lattice of MoS_2 while excess oxygen supplied by H_2O_2 was able to fill the lattice vacancies, due to the lower bonding affinity of Mo–S than Mo–O (as shown in Scheme 1a) [28,30]. The formation of Mo–O bonds could further confirmed by the FT-IR spectrum (Fig. 1f), and the three characteristic peaks of 986, 838, and 534 cm^{-1} in the FT-IR spectrum were attributed to the stretching vibration of Mo–O, which indicated the layered orthorhombic MoO_3 phase, the doubly coordinated oxygen (Mo–O–Mo) stretching mode of the Mo^{6+} ions, and the bending vibration of an oxygen atom linked to three Mo (Mo_3–O), respectively [32,33].

The absorption spectrum of the as-prepared MoO_x QDs reached maximum at 315 nm (Fig. 2), and the strong absorption between 200 and 400 nm was due to the charge transfer of Mo–O band in MoO_6^{6-} octahedron [34]. The light brown color of the obtained MoO_x QDs solution was in agreement with that of reduced MoO_3 (inset of Fig. 2) [35]. Similar to most photoluminescent semiconductor nanoparticles, MoO_x QDs also showed the excitation-dependent photoluminescence behavior and the emission peak red-shifted (from ~500 to ~570 nm) with the excitation wavelength varied from 300 to 525 nm (Fig. 2). Photoluminescence intensity of the MoO_x QDs increased and generated strong signal at 515 nm with λ_{ex} of 425 nm, and then decreased dramatically. The strong photoluminescence of MoO_x QDs around 515 nm was chalked up to the deep-level emissions caused by its surface defects, oxygen vacancies, Mo interstitials and Mo^{5+} ion associated with an oxygen vacancy as neighbor [7,20,36]. The MoO_x QDs solution emitted intense yellow photoluminescence under UV light (365 nm) (inset of Fig. 2), which is comparable to that of reported graphene quantum dots, carbon dots and MoS_2 quantum dots [23–25], and the absolute fluorescence quantum yield of MoO_x QDs was 1.35%. In order to obtain the best pthotoluminescence intensity, the concentration ratio of H_2O_2 to MoS_2 was optimized, which was

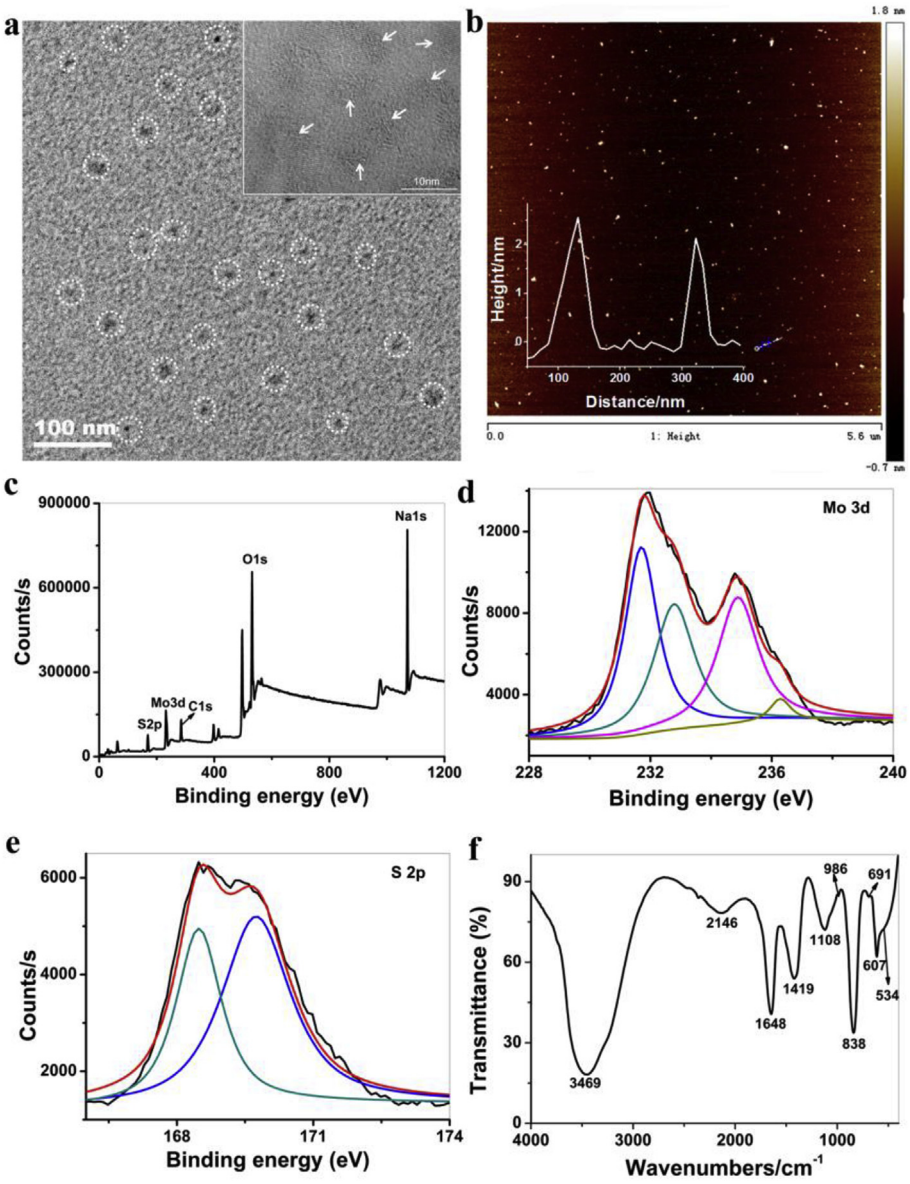

Fig. 1. (a) TEM images of the as-prepared MoO_x QDs that marked with circles. (b) AFM images of the as-prepared MoO_x QDs, and the insets demonstrated the corresponding height distributions. (c) is the XPS survey of the as-prepared MoO_x QDs while (d) and (e) are the high-resolution XPS spectra of Mo3d and S2p. (f) FT-IR spectrum of the as-prepared MoO_x QDs.

enhanced with the increasing concentration ratio of H_2O_2/MoS_2 and reached the highest value when the ratio of H_2O_2/MoS_2 was 50:3 (Fig. S4a). An optimal ratio of H_2O_2/MoS_2 = 50:3 was employed to guarantee the repeatability of the as-prepared MoO_x QDs. Besides, the comparable fluorescence intensity of various batches of MoO_x QDs indicated the good repeatability of the synthesis process (Fig. S4b), and the as-prepared MoO_x QDs maintained stablility in more than half a year at room temperature and no obvious change of photoluminescence intensity was observed when pH ranged from 2.0 to 12.0 (Fig. S5), suggesting the outstanding stability of MoO_x QDs to pH.

3.2. Quenched the photoluminescence of MoO_x QDs by Eu^{3+} ions

The above evidence demonstrated that the as-prepared MoO_x QDs is a new type of Mo-containing nanomaterial with excellent photoluminescence, which shows a strong photoluminescence peak around 530 nm when excited at 405 nm (Fig. 3a). In the presence of Eu^{3+} ions, however, Eu^{3+} ions were able to coordinate with oxygen atoms on the surface of MoO_x QDs, leading to dramatically decreased photoluminescence response. Sequential decreases of photoluminescence emission were observed in the presence of increasing amount of Eu^{3+} ions, and the oxygen atoms on the surface of MoO_x QDs got saturated with 275 μM Eu^{3+} ions when nearly 80% of the photoluminescence at 530 nm was quenched. The quenching could also be confirmed by visible color change (inset photograph in Fig. 3a). It should be note that a new peak around 610 nm gradually appeared when increasing amount of Eu^{3+} incubation with MoO_x QDs, could be account for the scattering signal of the formed MoO_x QDs–Eu^{3+} aggregates since the peak disappeared when excited at 450 nm (Fig. S6). The photoluminescence quenching mechanism of MoO_x QDs by Eu^{3+} ions might involved the following two aspects: ① Eu^{3+} ions quenched the photoluminescence of MoO_x QDs through energy transfer,

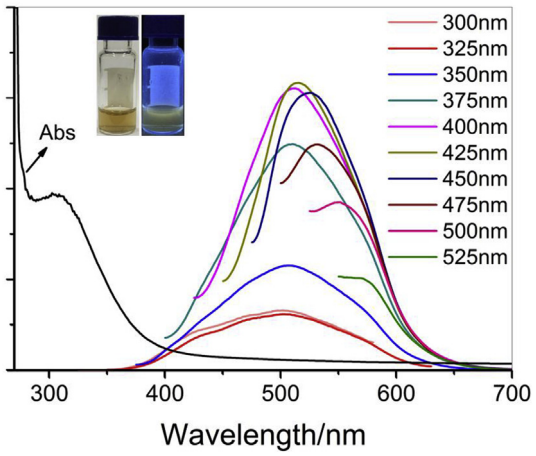

Fig. 2. The absorption (black line) and the excitation-dependent photoluminescence emission of the as-prepared MoO_x QDs. Inset photographs showed the color of MoO_x QDs solution under visible (left) and UV light at 365 nm (right). (For interpretation of the references to color in this figure legend, the reader is referred to the web version of this article.)

QDs -Eu^{3+} solutions were subjected to a 3 kDa MWCO ultrafiltration membrane, through which only Eu^{3+} in the solution while those adhered to the surface of MoO_x QDs could not pass, and the concentration of Eu^{3+} ions in the filtrate were determined by ICP-MS, as shown in Table S2. The Eu^{3+} ions in the filtrate were decreased from 60.2% (without MoO_x QDs) to 2.4% with addition of MoO_x QDs, demonstrating that Eu^{3+} ions are able to coordinate with oxygen atoms on the surface of MoO_x QDs, leading to the quenching of MoO_x QDs photoluminescence. The large MoO_x QDs nanoparticles was also observed by AFM (Fig. 4), the height of MoO_x QDs alone was about 2 nm, and that of MoO_x QDs-Eu^{3+} aggregates increased to 30–45 nm. Simply put, the photoluminescence quenching of MoOx QDs by Eu^{3+} ions was account for the photo-induced electron transfer mechanism and the disappearance of bright species.

3.3. The performance of the present off-on sensor for Pi detection

The binding affinity of Eu^{3+} ions to oxygen atoms was reported varied with the functional groups [39]. Since the binding affinity of Eu^{3+} ions to the oxygen atoms from the surface of MoO_x QDs might

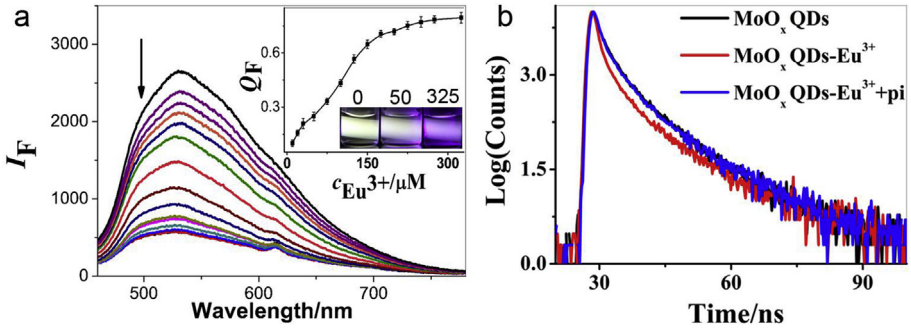

Fig. 3. (a) Photoluminescence of the MoO_x QDs quenched by increasing amount of Eu^{3+} ions. Concentration of Eu^{3+} ions from top to down is 0, 10, 20, 30, 50, 75, 100, 125, 150, 175, 200, 225, 250, 275, 325 μM, respectively. Inset is the photoluminescence responses at 530 nm titrated with Eu^{3+} ions. The inset picture shows the color change of the solutions excited at 405 nm. (b) Fluorescence lifetimes of MoO_x QDs, MoO_x QDs-Eu^{3+} complexes and MoO_x QDs-Eu^{3+}-Pi. The data were obtained from three parallel samples. (For interpretation of the references to color in this figure legend, the reader is referred to the web version of this article.)

which could be supported by the decreased fluorescence lifetimes of MoO_x QDs with the addition of Eu^{3+} ions and the restored fluorescence lifetimes in the presence of Pi (Fig. 3a and Table S1). For MoO_x QDs, the trapping of excitons might be facilitated by the oxygen vacancy, the aggregation of oxygen vacancies and Mo^{5+} ion associated with an oxygen vacancy as neighbor [36], and Eu^{3+} ions might disrupt the radiative recombination of excitons or self-trapped excitons (STEs), resulting in the decreased lifetime of MoO_x QDs with the addition of Eu^{3+} ions. Moreover, the fluorescence resonance energy transfer mechanism could be ruled out since the emission spectrum of MoO_x QDs did not overlap with the absorption of Eu^{3+} ions (Fig. S7), and the photo-induced electron transfer mechanism might be the main reason for the quenching of MoO_x QDs. ② Eu^{3+} ions was able to coordinate with oxygen atoms on the surface of MoO_x QDs leading to the aggregation of MoO_x QDs, and the formation of large non-fluorescent MoO_x QDs nanoprarticales consequently. In other words, the disappearance of bright species with a remaining population of MoO_x that were of comparable brightness was the main reason for photoluminescence quenching. The same quenching mechanism was also found in other nanoparticles, such as Ag nanocluster [37] and GQDs [38]. The formation of MoO_x QDs- Eu^{3+} conjugates and large MoO_x QDs nanoprarticales was also confirmed by the ultrafiltration experiments and AFM. For the ultrafiltration experiments, MoO_x be weaker than that from Pi, the addition of Pi will consequently lead to the desorption of Eu^{3+} from MoO_x QDs, resulting the recovering of MoO_x QDs photoluminescence emission. As shown in Fig. 5, the photoluminescence enhanced significantly with the titration of Pi and the photoluminescence recovered to 92.7% of the unquenched MoO_x QDs when Pi reached to 250 μM, which is comparable to or higher than those of other off-on sensors [40–44]. The photoluminescence restoration could also be observed under UV-light (inset of Fig. 5). To further explore the Pi's effect on the restoration of photoluminescence, the MoO_x QDs-Eu^{3+}-Pi solutions were subjected to a 3 kDa MWCO ultrafiltration membrane, through which only Eu^{3+} and Eu^{3+}-Pi complex free in the solution while those coordinated to the surface of MoO_x QDs could not pass, as shown in Table S2. The Eu^{3+} ions in the filtrate were increased from 2.4% (without Pi) to 62.3% upon addition of increasing amount of Pi to the MoO_x QDs-Eu^{3+} conjugate solution, which demonstrated that Pi intensively coordinated with Eu^{3+} ions and could remove Eu^{3+} from the surface of MoO_x QDs, leading to the restoration of MoO_x QDs photoluminescence. Eu^{3+} ions desorption from MoO_x QDs surfaces by Pi could also observed by AFM. From the AFM images, the height of MoO_x QDs-Eu^{3+} aggregates was 30–45 nm (Fig. 4) while that decreased to about 2 nm with the addition of Pi, and the MoO_x QDs-Eu^{3+} complexes disaggregated. The formed precipitates also became clear and transparent with the addition of

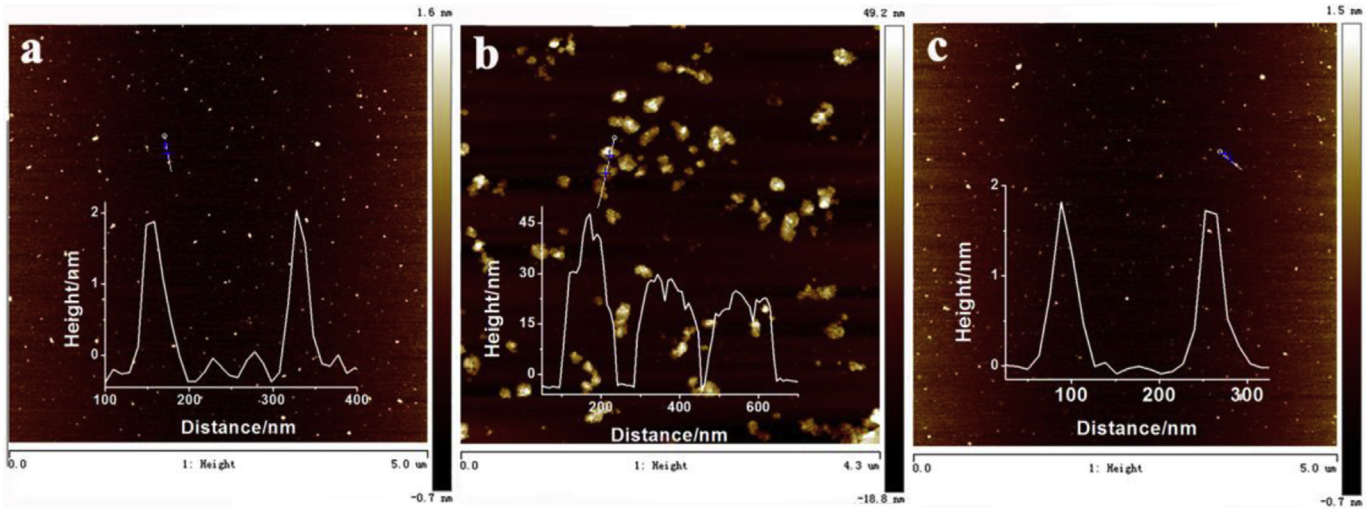

Fig. 4. AFM images of MoO_x QDs (a), MoO_x QDs+ 275 μM Eu^{3+} (b) and MoO_x QDs-Eu^{3+} in the presence of 150 μM Pi (c).

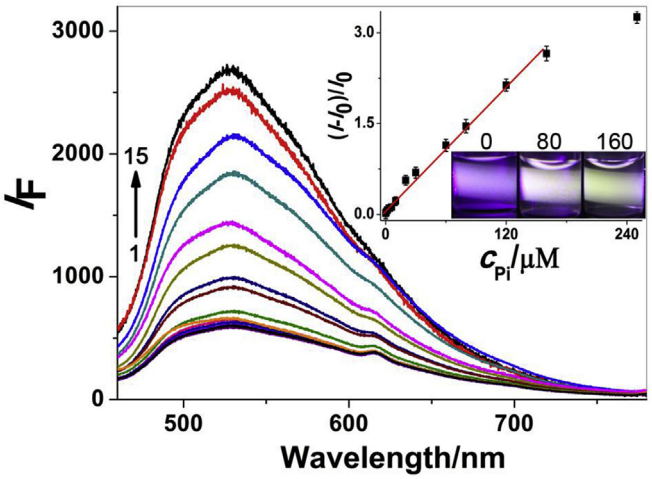

Fig. 5. The off-on photoluminescence spectra of MoO_x QDs-Eu^{3+}. The Pi concentration from 1 to 14 is 0, 0.1, 0.5, 2, 4, 6, 10, 20, 30, 60, 80, 120, 160, 250 μM respectively. 15 is the photoluminescence spectrum of MoO_x QDs. Inset is the fluorescence changes $(I-I_0)/I_0$ at 530.0 nm titrated with Pi. The inset picture shows the fluorescence restore of the MoO_x QDs-Eu^{3+} solutions excited at 405 nm. MoO_x QDs: 0.1 mg mL^{-1}; Eu^{3+}: 275.0 μM; 50 mM Tris–HCl buffer (pH 7.5); Ex: 405 nm. The data were obtained from three parallel samples.

Pi (Fig. S8).

Before applying the present sensor for Pi detection, the parameters including Eu^{3+} concentration, pH, reaction time and temperature of the sensor were optimized to the best performance. To ensure the photoluminescence quenching and recovery, the concentration of Eu^{3+} ions was optimized firstly in our experiments (Fig. 3a), and 275 μM was used in later experiments since the quenching efficiency reached the highest and no obvious precipitates were observed in such concentration. Since Eu^{3+} is a hard acid and can conjugate to the hard base OH^- to form insoluble $Eu(OH)_3$ species when pH > 8, and thus the quenching efficiency and the photoluminescence recovery might be influenced with pH. As showed in Fig. S9, the quenching efficiency increased when pH ranged from 6.0 to 7.0 and then decreased gradually While the photoluminescence recovery decreased when pH > 7.5, which accordance with the other reports that Eu^{3+} ions cannot coordinate to the oxygen atoms originated from targets when pH > 8.0 [41]. There force, the proposed sensor will performed at pH 7.5 in the later experiments to avoid the formation of insoluble $Eu(OH)_3$ species. Then, the reaction time and temperature were optimized (Fig. S10). The photoluminescence intensity of MoO_x QDs significantly increased during the early stages of the reaction and reached a plateau after 15 min, indicating that the Pi can selectively bind Eu^{3+} ions and remove them from the MoO_x QDs surfaces rapidly. Besides, the temperature-dependent experiments showed that the photoluminescence restoration of the present off-on sensor maintained stable from 15 °C to 40 °C, suggesting that Pi detection could be performed at room temperature. Under the optimized condition, the increased photoluminescence follows a linear equation of $(I-I_0)/I_0 = 0.05 + 0.02c$ (R = 0.99, n = 12) in the range of 0.1–160 μM with a detection limit of 56 nM (3σ/k), which is comparable to that of optical and electrochemical sensors (As shown in Table 1).

Considering the promising application of the new off-on sensor for Pi detection in complicated samples, the selectivity was evaluated using a variety of distractors, such as anions (SO_4^{2-}, SO_3^{2-}, S^{2-}, ClO^-), metal ions (Zn^{2+}, Cu^{2+}, Hg^{2+}, Fe^{2+}, Co^{2+}, Cd^{2+}, Ni^{2+}, Mn^{2+}), leucine (Leu), BSA and amylase (Amy). As seen in Fig. 6 and Fig. S11, only Pi caused a dramatic restoring of photoluminescence intensity, and the distracters generated quite weak photoluminescence restoration, illustrating that the proposed off–on photoluminescent MoO_x QDs-Eu^{3+} probe is especially selective to Pi ascribed to the strong and specific binding affinity of Eu^{3+} ions to Pi. It should also be noted that other phosphate containing compounds, such as ATP and PPi, also caused a dramatic restoration while organophosphate-dimethoate induced quite weak restoration (Fig. 6 and Fig. S11), which obey the sensing mechanism that the strong binding of Eu^{3+} to phosphate induce the disaggregation of MoO_x QDs-Eu^{3+} conjugates leading to the photoluminescence restoration of MoO_x QDs. Although PPi and ATP generated a dramatic increase, the interfere of PPi and ATP in Pi determination in real water samples can be ignored since orthophosphates is the major form of soluble phosphorus in natural water and other soluble phosphates like organic phosphates, pyrophosphate and polyphosphates are eventually hydrolyzed into orthophosphates [49].

3.4. Pi detection in lake water samples with the present off-on sensor

To validate the feasibility of the present off-on sensor, the

Table 1
Comparison of different methods for Pi determination.

Methods	Systems	Samples	Linear range (μM)	LOD (μM)	Reference
Fluorescence	CDs-Eu^{3+}	Artificial wetlands	0.4–150	0.05	[41]
Fluorescence	GQD-Eu^{3+}	Artificial wetlands	0.5–190	0.1	[38]
Fluorescence	Polyfluorene	Blood serum	–	4.8	[45]
Fluorescence	Mn:ZnTe/ZnSe QDs	Tap water	0.67–50	0.2	[46]
Amperometric-BIA	Three-electrode	Seawater	1–20	0.3	[47]
Naked-eye colorimetric	$[Zn_2$(H-bpmp)(pyrocatecholviolet)$]^+$	Water	–	10	[48]
Fluorescence	MoO_x QDs-Eu^{3+}	Lake water	0.1–160.0	0.06	This work

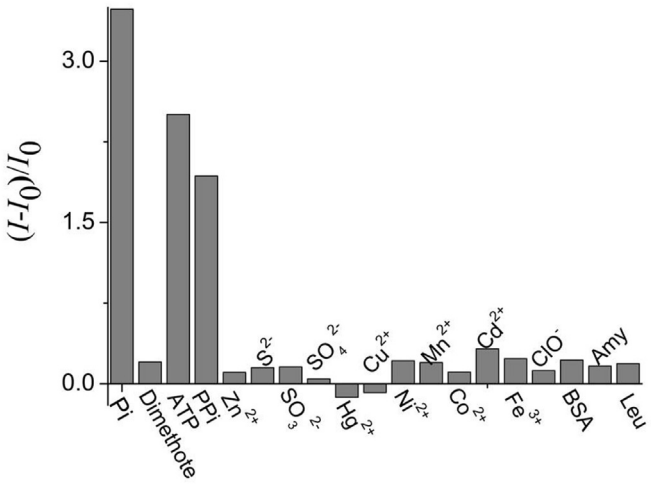

Fig. 6. Selectivity of the off-on assay based on the MoO_x QDs-Eu^{3+} photoluminescent probe for Pi over other substances. The concentration of Pi and other substrances was 160 μM. MoO_x QDs: 0.1 mg mL^{-1}; Eu^{3+}: 275.0 μM; 50 mM Tris–HCl buffer (pH 7.5); Ex: 405 nm; Em: 530 nm.

concentration of Pi in lake water was determined, and the results showed that Pi concentrations in two lake water samples were 13.78 and 8.91 μM (Table 2), which are well accordance with those obtained by the standard molybdenum-blue method, suggesting the high accuracy of the present off-on sensor. Moreover, the recovery (93.9 and 104.6%) and the standard deviations calculated from three parallel samples also demonstrated that the present off-on sensor has high accuracy and good repeatability, which are acceptable for Pi detection in lake water samples.

4. Conclusion

In conclusion, a facile method was developed for the synthesis of highly photoluminescent MoO_x QDs at room temperature without any external stimuli, and the as-prepared MoO_x QDs was employed as an efficient photoluminescent probe for Pi detection in lake water samples without any complex pretreatments, due to the excellent binding affinity of Eu^{3+} ions to Pi. MoO_x QDs, which is easily prepared, environment friendly and biocompatible, was used as a photoluminescent probe firstly for ion photochemical sensing, which opens the gate of employing MoO_x nanomaterials as a versatile photoluminescent probe in a variety of fields, such as chemi- and bio-sensors, cell imaging, biomedical and so on.

Acknowledgments

This work has been supported by the National Natural Science Foundation of China (Nos. 21205011 and 21465003), Program for Changjiang Scholars and Innovative Research Team in University (No. IRT13054), Opening Fund of State Key Laboratory Breeding Base of Nuclear Resources and Environment (No. NRE1314).

Appendix A. Supplementary data

Supplementary data related to this article can be found at http://dx.doi.org/10.1016/j.aca.2015.12.022.

References

[1] S. Bai, S. Chen, L. Chen, K. Zhang, R. Luo, D. Li, C.C. Liu, Ultrasonic synthesis of MoO_3 nanorods and their gas sensing properties, Sens. Actuat. B Chem. 174 (2012) 51–58.
[2] N. Illyaskutty, S. Sreedhar, G.S. Kumar, H. Kohler, M. Schwotzer, C. Natzeck, V.P.M. Pillai, Alteration of architecture of MoO_3 nanostructures on arbitrary substrates: growth kinetics, spectroscopic and gas sensing properties, Nanoscale 6 (2014) 13882–13894.
[3] S.N. Lou, N. Yap, J. Scott, R. Amal, Y.H. Ng, Influence of MoO3(110) crystalline plane on its self-charging photoelectrochemical properties, Sci. Rep. 4 (2014) 7428.
[4] Y. Wang, X. Zhang, Z. Luo, X. Huang, C. Tan, H. Li, B. Zheng, B. Li, Y. Huang, J. Yang, Y. Zong, Y. Ying, H. Zhang, Liquid-phase growth of platinum nanoparticles on molybdenum trioxide nanosheets: an enhanced catalyst with intrinsic peroxidase-like catalytic activity, Nanoscale 6 (2014) 12340–12344.
[5] M.A. Ibrahem, F.-Y. Wu, D.A. Mengistie, C.-S. Chang, L.-J. Li, C.W. Chu, Direct conversion of multilayer molybdenum trioxide to nanorods as multifunctional electrodes in lithium-ion batteries, Nanoscale 6 (2014) 5484–5490.
[6] Y. Shen, N. Xu, S. Deng, Y. Zhang, F. Liu, J. Chen, A Mo nanoscrew formed by crystalline Mo grains with high conductivity and excellent field emission properties, Nanoscale 6 (2014) 4659–4668.
[7] T. Anh Tran, K. Krishnamoorthy, Y.W. Song, S.K. Cho, S.J. Kim, Toxicity of nano molybdenum trioxide toward invasive breast cancer cells, ACS Appl. Mater. Interf. 6 (2014) 2980–2986.
[8] K. Krishnamoorthy, M. Premanathan, M. Veerapandian, S.J. Kim, Nanostructured molybdenum oxide-based antibacterial paint: effective growth inhibition of various pathogenic bacteria, Nanotech 25 (2014) 596–606.
[9] O. Lupan, V. Cretu, M. Deng, D. Gedamu, I. Paulowicz, S. Kaps, Y.K. Mishra, O. Polonskyi, C. Zamponi, L. Kienle, V. Trofim, I. Tiginyanu, R. Adelung, Versatile growth of freestanding orthorhombic alpha-Molybdenum trioxide nano- and microstructures by rapid thermal processing for gas nanosensors, J. Phys. Chem. C 118 (2014) 15068–15078.
[10] D. Xiang, C. Han, J. Zhang, W. Chen, Gap states assisted MoO_3 nanobelt photodetector with wide spectrum response, Sci. Rep. 4 (2014) 254.

Table 2
Detection results of Pi in lake water samples by the present off-on assay and the standard molybdenum-blue method.

Samples No.	The proposed off-on sensor				The molybdenum-blue method			
	Measured (Mean ± SD, n = 3, μM)	Value added (μM)	Value found (Mean ± SD, n = 3, μM)	Recovery (%)	Measured (Mean ± SD, n = 3, μM)	Value added (μM)	Value found (Mean ± SD, n = 3, μM)	Recovery (%)
1	13.78 ± 0.012	30.0	31.37 ± 0.072	104.6	13.92 ± 0.011	30.0	31.00 ± 0.013	103.3
2	8.91 ± 0.010	30.0	28.10 ± 0.011	93.7	8.85 ± 0.008	30.0	30.50 ± 0.012	101.7

[11] Y.L. Yang, Y. Shen, Z. Li, Reaction time effect of straw-like MoO_3 prepared with a facile, additive-free hydrothermal process, Rsc Adv. 5 (2015) 255–260.
[12] J. Yang, F. Lu, Y. Li, S. Yang, R. Li, N. Huo, C. Fan, Z. Wei, J. Li, S.-S. Li, Low temperature electrical transport and photoresponsive properties of H-doped MoO_3 nanosheets, J. Mater. Chem. C 2 (2014) 1034–1040.
[13] G. Song, J. Shen, F. Jiang, R. Hu, W. Li, L. An, R. Zou, Z. Chen, Z. Qin, J. Hu, Hydrophilic molybdenum oxide nanomaterials with controlled morphology and strong plasmonic absorption for photothermal ablation of cancer cells, ACS Appl. Mater. Interf. 6 (2014) 3915–3922.
[14] R.K. Sharma, G.B. Reddy, Controlled growth of vertically aligned MoO3 nanoflakes by plasma assisted paste sublimation process, J. Appl. Phys. 114 (2013) 184310–184317.
[15] I. Shakir, M. Shahid, U.A. Rana, M.F. Warsi, In situ hydrogenation of molybdenum oxide nanowires for enhanced supercapacitors, Rsc Adv. 4 (2014) 8741–8745.
[16] M.M.Y.A. Alsaif, S. Balendhran, M.R. Field, K. Latham, W. Wlodarski, J.Z. Ou, K. Kalantar-Zadeh, Two dimensional α-MoO_3 nanoflakes obtained using solvent-assisted grinding and sonication method: application for H_2 gas sensing, Sens. Actuat. B Chem 192 (2014) 196–204.
[17] R. Pandeeswari, B.G. Jeyaprakash, Nanostructured α-MoO3 thin film as a highly selective TMA sensor, Biosens. Bioelectron. 53 (2014) 182–186.
[18] D.Z. Pai, K. Ostrikov, S. Kumar, D.A. Lacoste, I. Levchenko, C.O. Laux, Energy efficiency in nanoscale synthesis using nanosecond plasmas, Sci. Rep. 3 (2013) 1221.
[19] L. Silipigni, F. Barreca, E. Fazio, F. Neri, T. Spano, S. Piazza, C. Sunseri, R. Inguanta, template electrochemical growth and properties of Mo oxide nanostructures, J. Phys. Chem. C 118 (2014) 22299–22308.
[20] I. Navas, R. Vinodkumar, V.P. Mahadevan pillai, Self-assembly and photoluminescence of molybdenum oxide nanoparticles, Appl. Phys. A 103 (2011) 373–380.
[21] M. Vila, C. Diaz-Guerra, D. Jerez, K. Lorenz, J. Piqueras, E. Alves, Intense luminescence emission from rare-earth-doped MoO_3 nanoplates and lamellar crystals for optoelectronic applications, J. Phys. D Appl. Phys. 47 (2014) 5880–5885.
[22] M. Maaza, B.D. Ngom, S. Khamlich, J.B. Kana Kana, P. Sibuyi, D. Hamidi, S. Ekambaram, Valency control in $MoO_{3-\delta}$ nanoparticles generated by pulsed laser liquid solid interaction, J. Nanopart. Res. 14 (2012) 1–9.
[23] H. Zhu, X. Wang, Y. Li, Z. Wang, F. Yang, X. Yang, Microwave synthesis of fluorescent carbon nanoparticles with electrochemiluminescence properties, Chem. Commun. (2009) 5118–5120.
[24] R. Liu, D. Wu, X. Feng, K. Müllen, Bottom-up fabrication of photoluminescent graphene quantum dots with uniform morphology, J. Am. Chem. Soc. 133 (2011) 15221–15223.
[25] Y. Wang, Y. Ni, Molybdenum disulfide quantum dots as a photoluminescence sensing platform for 2,4,6-trinitrophenol detection, Anal. Chem. 86 (2014) 7463–7470.
[26] J.H. Ryther, W.M. Dunstan, Nitrogen, phosphorus, and eutrophication in the coastal marine environment, Science 171 (1971) 1008–1013.
[27] H. Zhang, K.P. Loh, C.H. Sow, H. Gu, X. Su, C. Huang, Z.K. Chen, Surface modification studies of edge-oriented molybdenum sulfide nanosheets, Langmuir 20 (2004) 6914–6920.
[28] H.W. Wang, P. Skeldon, G.E. Thompson, XPS studies of MoS_2 formation from ammonium tetrathiomolybdate solutions, Surf. Coat. Tech. 91 (1997) 200–207.
[29] Q. Li, E.C. Walter, W.E. Van Der Veer, B.J. Murray, J.T. Newberg, E.W. Bohannan, J.A. Switzer, J.C. Hemminger, R.M. Penner, Molybdenum disulfide nanowires and nanoribbons by electrochemical/chemical synthesis, J. Phys. Chem. B 109 (2005) 3169–3182.
[30] N.M.D. Brown, N. Cui, A. Mckinley, An XPS study of the surface modification of natural MoS_2 following treatment in an RF-oxygen plasma, Appl. Surf. Sci. 134 (1998) 11–21.
[31] L. Dong, S. Lin, L. Yang, J. Zhang, C. Yang, D. Yang, H. Lu, Spontaneous exfoliation and tailoring of MoS_2 in mixed solvents, Chem. Commun. 50 (2014) 15936–15939.
[32] L.-L. Sui, Y.-M. Xu, X.-F. Zhang, X.-L. Cheng, S. Gao, H. Zhao, Z. Cai, L.-H. Huo, Construction of three-dimensional flower-like α-MoO3 with hierarchical structure for highly selective triethylamine sensor, Sens. Actuat. B Chem. 208 (2015) 406–414.
[33] J. Jiang, J. Liu, S. Peng, D. Qian, D. Luo, Q. Wang, Z. Tian, Y. Liu, Facile synthesis of [small alpha]-MoO_3 nanobelts and their pseudocapacitive behavior in an aqueous Li_2SO_4 solution, J. Mater. Chem. A 1 (2013) 2588–2594.
[34] T. Xia, Q. Li, X. Liu, J. Meng, X. Cao, Morphology-controllable synthesis and characterization of single-crystal molybdenum trioxide, J. Phys. Chem. B 110 (2006) 2006–2012.
[35] M. Dieterle, G. Weinberg, G. Mestl, Raman spectroscopy of molybdenum oxides Part I. Structural characterization of oxygen defects in MoO3-x by DR UV/VIS, Raman spectroscopy and X-ray diffraction, Phys. Chem. Chem. Phys. 4 (2002) 812–821.
[36] M. Itoh, K. Hayakawa, S. Oishi, Optical properties and electronic structures of layered MoO3 single crystals, J. Phys. Condens. Mat. 13 (2001) 6853–6864.
[37] L. Zhang, R.P. Liang, S.J. Xiao, J.M. Bai, L.L. Zheng, L. Zhan, X.J. Zhao, J.D. Qiu, C.Z. Huang, DNA-templated Ag nanoclusters as fluorescent probes for sensing and intracellular imaging of hydroxyl radicals, Talanta 118 (2014) 339–347.
[38] J.-M. Bai, L. Zhang, R.-P. Liang, J.-D. Qiu, Graphene quantum dots combined with europium ions as photoluminescent probes for phosphate sensing, Chem. A Eur. J. 19 (2013) 3822–3826.
[39] J. Hong, D. Pei, X. Guo, Quantum dot-Eu^{3+} conjugate as a luminescence turn-on sensor for ultrasensitive detection of nucleoside triphosphates, Talanta 99 (2012) 939–943.
[40] T. Wen, N.B. Li, H.Q. Luo, A turn-on fluorescent sensor for sensitive and selective detection of sodium dodecyl sulfate based on the eosin Y/polyethyleneimine system, Anal. Chem. 85 (2013) 10863–10868.
[41] H.X. Zhao, L.Q. Liu, Z.D. Liu, Y. Wang, X.J. Zhao, C.Z. Huang, Highly selective detection of phosphate in very complicated matrixes with an off-on fluorescent probe of europium-adjusted carbon dots, Chem. Commun. 47 (2011) 2604–2606.
[42] C. Lei, Z. Wang, Z. Nie, H.H. Deng, H.P. Hu, Y. Huang, S.Z. Yao, Resurfaced fluorescent protein as a sensing platform for label-free detection of dopper(II) ion and acetylcholinesterase activity, Anal. Chem. 87 (2015) 1974–1980.
[43] S.K. Lim, P. Chen, F.L. Lee, S. Moochhala, B. Liedberg, Peptide-assembled graphene oxide as a fluorescent turn-on sensor for lipopolysaccharide (endotoxin) detection, Analy. Chem. 87 (2015) 9408–9412.
[44] D. Zhao, Y. Fan, F. Gao, T.M. Yang, "Turn-off-on" fluorescent sensor for N-methyl-4 -pyridyl porphyri -DNA and G-quadruplex interactions based on nCdSe quantum dots, Anal. Chim. Acta 888 (2015) 131–137.
[45] A.K. Dwivedi, G. Saikia, P.K. Iyer, Aqueous polyfluorene probe for the detection and estimation of Fe^{3+} and inorganic phosphate in blood serum, J. Mater. Chem. 21 (2011) 2502–2507.
[46] Y. Song, Y. Li, Y.L. Liu, X.G. Su, Q. Ma, Highly sensitive and selective detection of phosphate using novel highly photoluminescent water-soluble Mn-doped ZnTe/ZnSe quantum dots, Talanta 144 (2015) 680–685.
[47] J.C. Quintana, L. Idrissi, G. Palleschi, P. Albertano, A. Amine, M.E. Rhazi, D. Moscone, Investigation of amperometric detection of phosphate: application in seawater and cyanobacterial biofilm samples, Talanta 63 (2004) 567–574.
[48] M.S. Han, D.H. Kim, Naked-eye detection of phosphate ions in water at physiological pH: a remarkably selective and easy-to-assemble colorimetric phosphate sensing probe, Angew. Chem. Int. Ed. 41 (2002) 3809–3811.
[49] V.K. Athanasios, K.K. Dimitrios, E.B. Craig, Rapid and portable electrochemical quantification of phosphorus, Anal. Chem. 87 (2015) 4269–4274.